

Interpreting artificial neural networks to detect genome-wide association signals for complex traits

Burak Yelmen^{1,*}, Maris Alver¹, Estonian Biobank Research Team¹, Flora Jay², Lili Milani¹

1 Estonian Genome Centre, Institute of Genomics, University of Tartu, Tartu, Estonia

2 CNRS, INRIA, LISN, Paris-Saclay University, Orsay, France

*burak.yelmen@ut.ee

Abstract

Investigating the genetic architecture of complex diseases is challenging due to the highly polygenic and interactive landscape of genetic and environmental factors. Although genome-wide association studies (GWAS) have identified thousands of variants for multiple complex phenotypes, conventional statistical approaches can be limited by simplified assumptions such as linearity and lack of epistasis models. In this work, we trained artificial neural networks for predicting complex traits using both simulated and real genotype/phenotype datasets. We extracted feature importance scores via different post hoc interpretability methods to identify potentially associated loci (PAL) for the target phenotype. Simulations we performed with various parameters demonstrated that associated loci can be detected with good precision using strict selection criteria, but downstream analyses are required for fine-mapping the exact variants due to linkage disequilibrium, similarly to conventional GWAS. By applying our approach to the schizophrenia cohort in the Estonian Biobank, we were able to detect multiple PAL related to this highly polygenic and heritable disorder. We also performed enrichment analyses with PAL in genic regions, which predominantly identified terms associated with brain morphology. With further improvements in model optimization and confidence measures, artificial neural networks can enhance the identification of genomic loci associated with complex diseases, providing a more comprehensive approach for GWAS and serving as initial screening tools for subsequent functional studies.

Keywords: Deep learning, interpretability, genome-wide association studies, complex diseases

Introduction

Understanding the genetic component of complex diseases is challenging due to high polygenicity and confounding factors defining these traits. Genome-wide association studies (GWAS) have been crucial for the discovery of thousands of disease-related genomic loci in the past two decades [1], and they continue to be relevant thanks to ever-expanding biobanks with deep phenotype/genotype datasets, allowing the detection of the most minuscule but statistically significant signals. Despite the immense success and broad applications over all types of traits, conventional GWAS methodology still relies on linear models (i.e., logistic and linear regression) for detecting such signals. More recently, linear mixed models have been utilised to incorporate random and fixed effects, especially to account for relatedness and population structure without data pruning [2, 3]. Although such improvements seem to improve GWAS outcomes generally, they do not diverge from the fundamental assumptions of linear and additive genetic models for complex traits. A natural alternative for the nonlinear modelling of such traits would be machine learning, and especially deep learning, since sufficiently large neural networks can approximate any bounded continuous function as defined in the universal approximation theorem [4]. Hence, not surprisingly, various models have been developed for the prediction of disease status from genetic data following the success of deep learning applications in many domains [5, 6]. Despite the state-of-the-art performance of these models in prediction, a main drawback of utilising such complex architectures is the inherent difficulty of interpretability due to the high number of parameters at various abstraction levels. In this context, the development and integration of interpretability methodology are not only important for understanding model biases and improving architectures but also for detecting novel features (e.g., genomic loci, haplotypes, or variants) associated with the target phenotype. Various approaches have been proposed to tackle interpretability for the potential discovery of causal genomic loci, ranging from intrinsically interpretable architectures based on domain knowledge, such as functional gene annotations [7, 8, 9], to post hoc analysis of trained models [10, 11, 12, 13]. Despite these important advancements, multiple challenges remain for the widespread use of interpretable deep learning in genomics. For instance, many of the proposed methods rely on either specific architectures, specific interpretability methods, or a priori biological knowledge. In this work, **(i)** we propose a general framework for obtaining potentially associated loci (PAL) from neural network models trained for phenotype prediction, **(ii)** compare the performance of different post hoc and model-agnostic interpretability methods and logistic regression using simulations and **(iii)** apply our approach to the Estonian Biobank (EstBB) [14] schizophrenia (SCZ) cohort demonstrating its utility for GWAS and reporting potentially novel loci not reported in literature.

Materials and Methods

Data

We assembled the SCZ cohort from the EstBB dataset so that all patients (ICD codes F20-F29) would have at least one antipsychotic prescription and have their first diagnosis after 2006 with the diagnosis age between 14 and 60. For SCZ cases, we first assembled a set of individuals without any mental, behavioural and neurodevelopmental disorders (no ICD F* diagnosis) and without any antipsychotic prescription. From this filtered set, controls were selected to match the age, sex and BMI distribution of the case cohort with four controls per case using MatchIt [15]. We used exact matching (method = “exact”) for sex and nearest neighbour matching (method = “nearest”) for BMI and age, resulting in 1814 cases (642 male, 1172 female) and 7325 controls (2586 male, 4739 female). In addition, the whole dataset was pruned to eliminate relatedness based on identity by descent ($\pi_{\text{hat}} < 0.2$). We curated the genotype data of the EstBB SCZ case/control cohort derived from the GSA array (Illumina’s GSA-MD-24v1, GSA-MD-24v2, ESTchip1_GSA-MD-24v2, ESTchip2_GSA-MD-24v3, 2022-09-14 snapshot) with a final set of 290,522 SNPs over 22 autosomal chromosomes after removing SNPs unique to at least one version of the array, indels and filtering for bi-allelic regions.

Simulations

We obtained the simulated phenotypes from the same combined SCZ case/control genotype dataset. Instead of simulating genotypes, we simulated phenotypes to keep genome distribution as realistic as possible. More in detail, let X represent the genotype matrix where X_{ij} is the genotype at position j for individual i with possible values -1 (AA), 0 (AB), 1 (BB); β the vector of genetic weights sampled from standard normal distribution $N(0,1)$; ϵ_i the noise term sampled from $N(0, k\sigma^2)$ where k is a scaling factor and σ^2 is the variance of the total genetic effects. Then the continuous phenotype Y for individual i is defined as:

$$Y_i = \sum_{j \in D} f_j^D(X_{ij}) + \sum_{j \in R} f_j^R(X_{ij}) + \sum_{(j,k) \in I} f_{jk}(X_{ij}, X_{ik}) + \sum_{(j,k,l) \in I} f_{jkl}(X_{ij}, X_{ik}, X_{il}) + \epsilon_i$$

where the initial four terms define the genetic effects based on dominant, recessive, two-way (between 2 SNPs) and three-way (between 3 SNPs) interactions; D , R and I are disjoint sets of genomic positions for dominant, recessive and interaction effects. For dominant and recessive effect positions, contribution to the phenotype is defined by functions f_j^D and f_j^R :

$$f_j^D(X_{ij}) = \begin{cases} \beta_j \cdot X_{ij} & \text{if } X_{ij} \neq -1 \\ 0 & \text{otherwise} \end{cases}$$

$$f_j^R(X_{ij}) = \begin{cases} \beta_j \cdot X_{ij} & \text{if } X_{ij} = 1 \\ 0 & \text{otherwise} \end{cases}$$

Two-way and three-way interaction effects are defined by:

$$f_{jk}(X_{ij}, X_{ik}) = \beta_{jk} \cdot X_{ij} \cdot X_{ik}$$

$$f_{jkl}(X_{ij}, X_{ik}, X_{il}) = \beta_{jkl} \cdot X_{ij} \cdot X_{ik} \cdot X_{il}$$

Given a defined threshold τ , the continuous phenotype is then binarized by:

$$B_i = \begin{cases} 1 & \text{if } Y_i > \tau \\ 0 & \text{otherwise} \end{cases}$$

In practice, we chose τ to have approximately the same number of cases (~ 1814) as the real SCZ cohort. We simulated a total of 6 scenarios with different noise scaling factors ($k = 1, k = 2, k = 3$) and two different causal SNP sizes ($n = 100$ and $n = 1000$) where all four genetic effect types (dominant, recessive, two-way and three-way interactive) had positions with ratios 5:5:8:2, respectively (i.e., for $n = 100$: 40, 10, 25, 25 and for $n = 1000$: 400, 100, 250, 250). Genotypes were represented by -1, 0, 1 instead of 0, 1, 2 to provide equal importance to either allele in a given position (considering the neural network weights are initialised with Kaiming uniform distribution, including negative and positive values uniformly). Nevertheless, our preliminary trials with 0, 1, 2 representation provided similar results in terms of model training.

Neural network model

Models trained for binary trait classification were all feed forward fully connected neural networks with an input layer, two hidden layers and an output layer. The specific architecture consists of an initial dropout layer to randomly mask a proportion of features ($p = 0.99$) at each batch training, a linear layer with input size = 290,522 and output size = 290, a dropout layer ($p = 0.6$) followed by ReLU activation, a linear layer with input size = 290 and output size = 29, a dropout layer ($p = 0.6$) followed by GELU activation, a linear layer with input size = 29 and output size = 1 followed by sigmoid activation function. Training was performed using cross-entropy loss function and Adam optimizer with learning rate = $1e-5$ and weight decay = $1e-3$ for regularisation. Initially, we tried a weighted loss function to

compensate for the class imbalance in the real dataset but this did not work (i.e., no training run where the validation loss decreases), so we instead duplicated the case samples and reduced the sample size of the controls by half with random subsampling to match the case/control numbers [16]. We additionally added random noise $N(0,0.1)$ both to class labels (case label = 1, control label = 0) and input genotypes to increase generalizability. All models were trained for 1000 epochs with batch size = 256. All models were coded with python-3.9 and pythorch-1.11 [17].

Interpretability methods

There is a plethora of different interpretability methods for deep learning models, but we focused on three post hoc and model agnostic approaches. Two of them, gradients w.r.t input (saliency maps, SM) [18] and integrated gradients (IG) [19], are based on gradients and applicable to any differentiable model. SM creation is a commonly used and straightforward approach where gradients w.r.t input are obtained to assess which features in a given input are important for the output probability. For a binary classification neural network model f and input vector x , the saliency (with absolute values) for the j^{th} feature is defined as:

$$SM_j(x) = \left| \frac{\partial f(x)}{\partial x_j} \right|$$

IG is an improvement over the simpler gradient approach where gradients of the model’s output with respect to the input are integrated along a path from a baseline input to the actual input. For a neural network model f , input vector x , baseline x' and scalar $\alpha \in [0, 1]$, integrated gradient for the j^{th} feature is defined as:

$$IG_j(x) = (x_j - x'_j) \int_0^1 \frac{\partial f(x' + \alpha(x - x'))}{\partial x_j} d\alpha$$

As the authors of the method emphasise, the choice of baseline vector is important so that a meaningful interpolation can be achieved in the given domain. In our application, we tested various baselines and decided on using a vector of zeros (where the input is a case genotype) which in preliminary analyses, provided better outcomes compared to **(i)** [input = case and control genotypes] - [baseline = vector of average allele dosages for the whole dataset] and **(ii)** [input = case genotypes] - [baseline = control genotypes] settings. In this regard, our choice of genotype representations with -1, 0, 1 might also have been helpful since a vector of zeros would correspond to a completely heterozygous genome, without preference over any allele in a given position. We used Captum-0.6.0 python library [20] for calculating SM and IG.

Permutation-based feature importance (PM) is another model-agnostic technique (in this case, the model does not even need to be differentiable) that measures the impact of feature perturbations on model output [21]. For a neural network model f , input vector x and perturbed input vector $x^{(j)}$ (where the j^{th} feature is replaced by a random feature), the permutation feature importance for the j^{th} feature is defined as:

$$PM_j(x) = \left| f(x) - f(x^{(j)}) \right|$$

Here, we opted to measure the rate of change in predictions for the feature importance instead of a performance metric such as accuracy to increase sensitivity.

Using these three methods, we obtained absolute feature importance scores for a set of case samples (both in real and simulated scenarios) for all trained models, averaged the scores over samples and applied min-max normalisation to map the values to [0,1] range. We call this averaged value mean attribution score (MAS). Moreover, the obtained case set consisted of genotypes with neural network predicted probabilities above the 70th percentile. This thresholding was performed mainly for computational ease but also for utilising case samples with prediction values closer to 1. Different percentile thresholds and using all true case genotypes provided similar results in preliminary analyses.

Feature importance to potentially associated loci

To account for the stochasticity of neural networks and reduce false positive rate, we devised a streamlined method for obtaining potentially associated loci (PAL) from the MAS computed from multiple models trained with different seeds. More specifically, let A be the MAS matrix sized $m \times L$ where m is the number of models (i.e., models trained with different seeds) and L is the length of the genotype. We obtain the average MAS vector μ :

$$\mu = (\mu_1, \mu_2, \dots, \mu_L)$$

where

$$\mu_j = \frac{1}{m} \sum_{a=1}^m A_{aj} \quad \text{for } j = 1, 2, \dots, L$$

Then we set a significance threshold θ and obtain weights w based on the number of occurrences above the θ threshold among m models trained with different seeds:

$$w_j = \frac{1}{m} \sum_{a=1}^m \mathbf{1}(A_{aj} > \theta), \quad \text{where } \mathbf{1} \text{ is the indicator function}$$

To obtain PAL, first we define the adjusted mean attribution score (AMAS) as:

$$AMAS_j = w_j \cdot \mu_j, \quad \text{for all } j \text{ such that } \mu_j > \theta$$

Then the PAL set contains all positions above the theta threshold based on their AMAS:

$$PAL_{AMAS} = \{j \mid AMAS_j > \theta\}$$

We can also define PAL as positions above the theta threshold in all m models:

$$PAL_{Common} = \{j \mid \forall a, A_{aj} > \theta\}$$

In practice, we chose $m = 10$ for models trained with different seeds to be able to perform a large number of trials with realistic computational resources. Since there were multiple PAL in high LD detected by models trained with different seeds, we also considered these positions ($r^2 > 0.5$) between different models as common signals between models to increase detection power both for PAL_{Common} and PAL_{AMAS} . Furthermore, we set θ to 99.99 percentile (strict) and 99.95 percentile (relaxed) thresholds. Although the choice of θ is essentially arbitrary, the strict threshold produces 30 PAL and the relaxed threshold 145 PAL, which are plausible numbers for keeping the false positive rate low considering the expected high polygenicity of schizophrenia [22]. An overview of our proposed approach is provided in Fig 1.

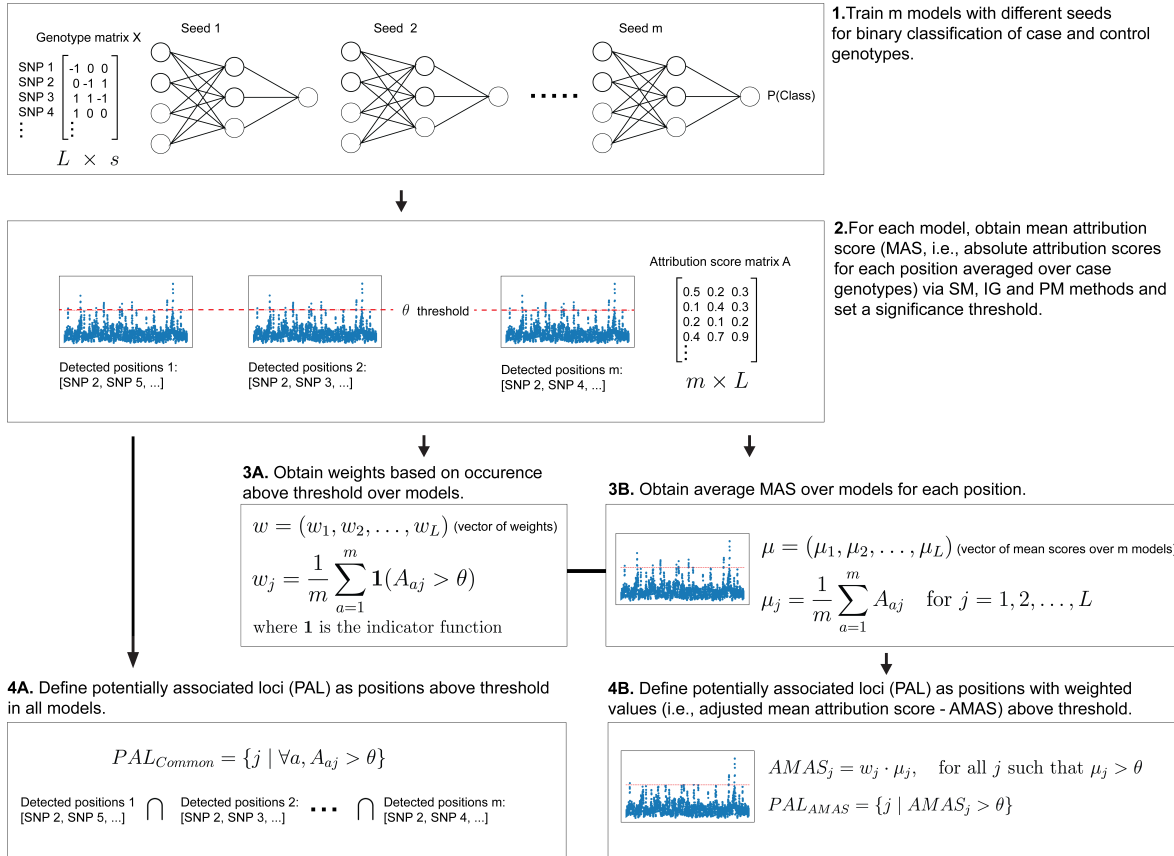


Figure 1. Overview of the approach for obtaining potentially associated loci (PAL) from feature attribution scores obtained via SM, IG and PM methods.

Logistic regression

To compare our method to conventional GWAS, we performed logistic regression (LR) using all case ($n = 1814$) and control ($n = 7325$) samples (both in real and simulated scenarios) using the top 3 principal components (PCs) from principal component analysis (PCA) as covariates. We obtained the significance threshold by dividing $p\text{-value} = 0.05$ by the number of tests (i.e., number of SNPs: 290,522). We used python-3.9 and statsmodels 0.14.1 [23] for the code. Furthermore, we performed an association analysis using REGENIE v2.2.4 [3] on real data with the same case/control genotypes via the methodology described by Pujol Gualdo et al. [24], except for the filtering steps to retain exactly the same individuals and positions as LR.

Relevant code for the neural network model, interpretability methods and logistic regression with mock simulated data can be found at <https://github.com/genodeco/Interpreting-ANNs-for-GWAS>.

Results

Simulations

For 6 different phenotype simulations with different noise scaling factors ($k = 1, k = 2, k = 3$) and different numbers of causal SNPs (100 and 1000 causal SNPs), we tested the performance of logistic regression (LR), saliency map (SM), integrated gradient (IG) and permutation-based (PM) feature importance approaches based on precision and ability to detect different types of causal positions (interaction and dominant/recessive). An important note here is that we defined true positive (TP) as a

detected position (i.e., PAL) which is in high correlation ($r^2 > 0.5$ in 100 SNP upstream and 100 SNP downstream region, total $\sim 2\text{Mb}$) with any true causal position (since high LD, which is prevalent in proximal loci, makes it difficult to detect the exact causal SNP). The results show that LR with Bonferroni correction seems to produce the least number of false positives over all different simulations but PAL_{AMAS} and PAL_{Common} obtained from the IG approach with strict thresholding (99.99 percentile) was a close contender (S1 Fig). Interestingly but perhaps expectedly, the LR approach predominantly detected the causal positions with interactive genetic effects, whereas the highest percentage of dominant/recessive positions were detected by gradient-based approaches (Table 1). We furthermore visualised the performance of IG on Manhattan plots obtained from LR (S2 Fig). Even under high noise schemes, some high-effect positions were detected both by LR and our method.

Table 1. Percentage of dominant/recessive positions (as opposed to interactive positions) in correctly detected causal loci averaged over all 6 simulation scenarios with varying parameters. Significance-based detection refers to Bonferroni correction for LR (logistic regression) and strict threshold (99.99 percentile) for IG (integrated gradients), SM (saliency map) and PM (permutation-based) approaches. Since significance thresholds are not directly comparable between LR and other methods, percentages were also provided for the top 5 and top 10 correctly detected causal loci. The expected frequency for dominant/recessive positions based on the phenotype simulations is 0.5. Values in parentheses demonstrate counts as [dominant/recessive]/([dominant/recessive] + [interactive]).

Category	Top 5	Top 10	Significance-based
LR	0.0000 (0/24)	0.0213 (1/47)	0.0902 (12/133)
IG	0.1304 (3/23)	0.2143 (9/42)	0.1268 (9/71)
SM	0.0000 (0/23)	0.1500 (6/40)	0.1549 (11/71)
PM	0.0500 (1/20)	0.1579 (6/38)	0.1618 (11/68)

Application to the EstBB SCZ cohort

After testing our approaches on simulations, we applied the IG method on the EstBB SCZ cohort to detect PAL. Although it is difficult to compare the methods reliably (see Discussion), we decided not to use SM and PM on real data due to higher false positives under certain simulation scenarios (S1 Fig). We detected a single locus with the strict threshold and multiple loci with the relaxed threshold in genomic regions with multiple protein-coding genes (Fig 2). The highest confidence signal on chromosome 4 (PAL d) included variants within *TET2* and *PPA2* genes and rs10010325 SNP, which has been reported to have pleiotropic effects for attention deficit hyperactivity disorder, autism spectrum disorder and intelligence [25]. Furthermore, in this LD region resides rs7674220 (albeit not being present in our non-imputed array framework), which is associated with SCZ and mapped to *TET2* [26]. Interestingly, rs2647259 present in this region in our data seems to be associated with *PPA2* expression levels in brain tissues (based on variant-gene association analysis, explained in the next paragraph). Other high-confidence regions we detected in chromosomes 3 (PAL c) and 11 (PAL f) are gene-dense regions with multiple low p-value SNPs in Trubetskoy et al. metadata (i.e., largest SCZ GWAS meta-analysis to date) [27]. The high signal LD region we detect in chromosome 11 includes rs1892928 (not present in our non-imputed array data), which was reported to be associated with SCZ and mapped to *SYT12*. In this region, we also detected rs7122539 (present in our array framework), which was shown to be associated with bipolar disorder and mapped to *PC* gene [28, 29]. The region in chromosome 3 includes rs4955417 (associated with depressive symptoms and neuroticism, mapped to *IHO1* and *C3orf62* [30, 31]) and rs7617480 (associated with major depressive disorder and unipolar depression [32, 33, 34]). Furthermore, *QRICH1* gene reported in the Schizophrenia Exome Sequencing Meta-Analysis (SCHEMA) with p-value < 0.01 and reported to be associated with developmental disorders and autism spectrum disorder resides in this region [35, 36, 27, 37]. Other lower confidence but potentially interesting regions include *C1orf87* (PAL a) (with gene ontology annotation calcium ion binding), and *AOX1* (PAL b) (with gene

ontology annotations oxidoreductase and electron transfer activity) genes. SNPs in detected PAL are presented in S1 Table, genes in detected PAL are presented in S2 Table, and SNPs with low p-values (<0.001) from Trubetskoy et al. 2022 metadata in detected high LD regions are presented in S3 Table.

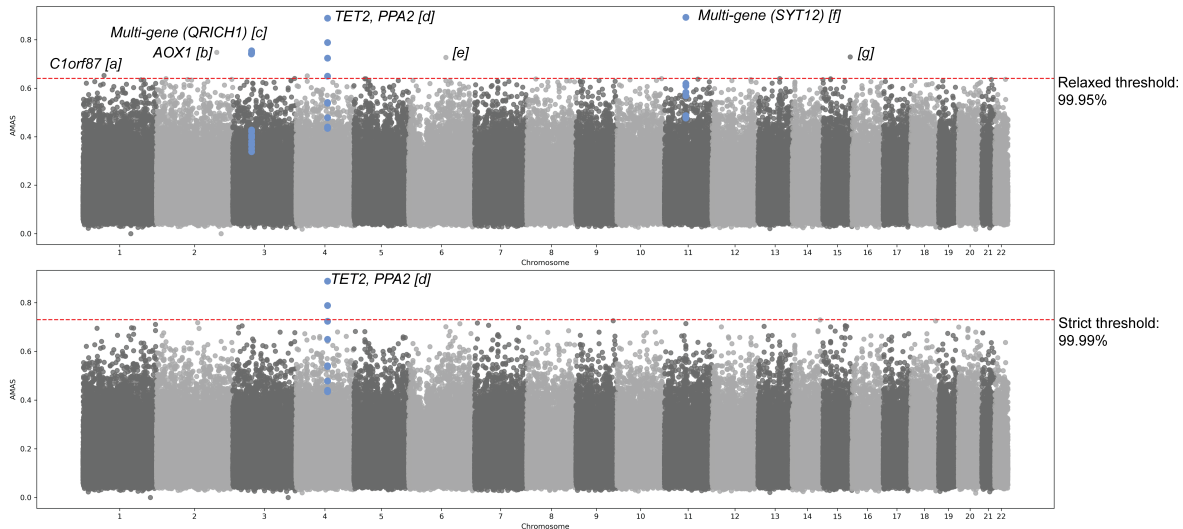


Figure 2. PAL detected by integrated gradients (IG) approach. Red dashed lines indicate significance thresholds (relaxed and strict) and blue markers indicate PAL above threshold over all trained 10 models (i.e., PAL_{Common}). For all PAL (a-g), protein coding genes in those regions were provided except for multi-gene regions (>2 genes) for which the most likely mapped gene based on literature was provided inside the parentheses.

We further assessed whether variants in the PAL we detected were enriched in genes with brain associations. For this purpose, we used the open access Adult Genotype Tissue Expression (GTEx) Project [38] variant-gene association dataset (GTEx_Analysis_v8_eQTL). Since we did not fine map the causal variants, we assessed the significant expression levels (significance defined as $pval_nominal < pval_nominal_threshold$ in significant variant-gene pairs dataset from GTEx

*.signif_variant_gene_pairs.txt.gz files) in all brain tissues for all detected loci and close proximity loci (100 SNP upstream and 100 SNP downstream region of the PAL, total ~2Mb) with high LD (>0.5). We initially obtained the empirical cumulative distribution function (ECDF) for significant gene-tissue (only brain tissues) expression change in all 290,522 positions. Mean value for all positions was 0.858 (i.e., on average, a SNP had 0.858 gene-tissue combinations with significantly altered expression in brain) with most positions (250,692 SNPs) having no variants significantly affecting gene expression in brain tissues. Percentile ranks for all methods detecting PAL was higher than 90, indicating potential enrichment in brain expressed genes in these detected regions (S3 Fig). As an additional step, we used the GENE2FUNC tool in FUMA [39] to assess functionality for the set of genes present in the detected PAL. In terms of expression, there was significant downregulation in brain tissues and in terms of GWAS enrichment, lowest enrichment p-values were related to brain morphology and volume with multiple involved genes (S4 Fig). It is important to note here that we directly tested all the genes in PAL without any gene mapping attempt, with most genes coming from gene-rich loci from chromosomes 3 and 11 (PAL c and f), which might potentially be introducing bias to these results. Another potential biasing caveat for both ECDF and functional analysis is that detected PAL generally consist of multiple SNPs in high LD, and it is likely that only a small portion of SNPs in these LD blocks indicate a true signal.

We furthermore compared these approaches with conventional GWAS using LR and REGENIE association analysis on the real dataset. Although there was a high correlation between MAS and $-\log(p)$ values (S5 Fig), there was no significant signal detected using GWAS, and only a single PAL overlap was

present in the top 10 signals (S6 Fig).

Discussion

In this work, we assessed post hoc neural network interpretability methods for detecting disease-associated genomic loci and proposed a general framework for using these methods within a genotype-phenotype context. Simulations demonstrated that these approaches can provide low false positive rates with strict thresholding even under relatively low genetic signal scenarios. An important note here is that the noise factor of 3 in simulations approximately corresponds to the SNP-based heritability estimate for SCZ, which is around 0.25 [27]. However, this estimate is based on linear additive models, whereas our simulated traits were based on interactive and dominant/recessive effect positions, possibly making detection of associated loci substantially more difficult. This brings us to a fundamental challenge in method development for causal detection, which is the lack of ground truth disease models. Without knowing the exact disease models, it is not trivial to assess these methods due to the likely discrepancy between simulated and real domains. In this regard, a potential solution, knockoff variables, has been adopted for neural networks in previous works [40, 13, 10]. Briefly, these are implanted “fake” positions following the distribution of the real input features to assess the false positive rates when detecting relevant features. However, sampling knockoff variables is not straightforward because deviations from the distribution of real input features would bias the false positive estimates. Furthermore, implementing a sufficient number of knockoff variables would potentially deteriorate the realness of data and significantly increase the computational burden due to the fully connected architecture of our models. Future parameter-light architectures (such as convolutions) could be more suitable to explore this approach. Another challenge for method assessment arises due to LD. Even through simulations with ground truth information, evaluation metrics such as TP/FP counts can be substantially biased since methods (including LR) tend to present highly correlated signals. With our definition of TP (i.e., a detected position in high correlation with any true causal position), a method might present higher TP (or FP) counts simply due to multiple signals in a high LD block as opposed to another method with signals consisting of isolated SNPs. Another LD-related challenge (but specific to our application) is due to models trained with different seeds detecting different signals in high LD. To increase our power, we counted these high LD PAL as common signals between models, which boosted TP signals in simulation analyses (S1 Fig). Although a substantial portion of this boost was probably due to overlapping signals, the same TP/FP analysis where we only considered exact detected SNPs as common between models demonstrated that our initial approach (common signals based on LD) allows catching more TP signals and FP signals do not change substantially between two approaches for the IG method (S7 Fig). Considering all these issues, future research might benefit from evaluation metrics better tailored for genomic data.

Another important subject related to neural networks is stochasticity. In our approach, we employed both heavy dropout regularisation (including unusual dropout masking before the input layer) and ensemble-like multiple seed training to take advantage of stochasticity and limit false positives. Interestingly, even with this heavy regularisation, we were able to train models successfully (i.e., positive correlation between training and validation loss), even though the predictive power of these models was limited. Receiver operating characteristic (ROC) curves for phenotype prediction in the real dataset were comparable between neural network and logistic regression models, with logistic regression being marginally better (S8 Fig). Initially, this might suggest that the real dataset primarily exhibits linear effects. Yet, as a counter-evidence to the “mainly linear effects” scheme, logistic regression could not detect any significant positions when applied to the real cohort, and there was no correspondence between the top detected positions of logistic regression and neural network approaches (S6 Fig), which might suggest the existence of nonlinearities in the real dataset. These aspects of effect types and how heavy regularisation alters the capacity of neural networks for detecting nonlinearities are interesting subjects for future research. Considering the relatively small dataset for a case/cohort type analysis in this work, increasing the training data and experimenting with more simulation scenarios (such as including more nonlinearities, gene-environment interactions or covariate effects) could be helpful to

distinguish the differences between linear and nonlinear approaches.

An intriguing finding was that all approaches mainly detected positions with interactive effects while neural network methods detected more positions with dominant/recessive effects compared to LR. This is potentially due to dominant/recessive positions being more difficult to detect since the SNP effect completely disappears for a proportion of genotypes (see Materials and Methods). Another related point is that the outcome space of functions defining the disease genomics is considerably smaller due to the ternary nature of the genotype variables. Research on the topology of this space could provide valuable insights on limitations of methods developed for in silico detection of causal loci and provide better roadmaps during development.

Despite the state-of-the-art deep learning algorithms and the ever-increasing amount of data in biobanks, there are still multiple challenges to the wide-spread adoption of neural networks for GWAS, such as stochasticity stemming from initial random states, lack of established uncertainty quantification and lack of ground truth disease models. These challenges are also fundamentally connected to very interesting questions, such as the contribution of nonlinear effects (gene-gene or gene-environment interactions or other polynomial disease models) or omnigenic vs polygenic models for complex disease development [41]. In the near future, assumption-free interpretable neural networks can become important tools to explore these questions and potentially replace linear models as the conventional method of conducting GWAS and obtaining interpretable polygenic risk scores.

Acknowledgements

BY, MA, LM were supported by the European Union's Horizon 2020 Research and Innovation Programme under Grant agreements No 964874 Realment and 847776 CoMorMent. Thanks to the Agence Nationale de la Recherche (ANR-20-CE45-0010-01) for funding. Thanks to the High Performance Computing Center (HPC) of the University of Tartu for providing computational resources. Thanks to the Estonian Biobank Research Team (Andres Metspalu, Tõnu Esko, Reedik Mägi, Mari Nelis, Georgi Hudjashov) for the genotype and phenotype datasets used in this work. Thanks to Liis Karo-Astover for administrative support and proofreading. Data used for the gene-variant expression analyses described in this manuscript were obtained from the Genotype-Tissue Expression (GTEx) Portal on 04/04/2024.

Contributions

Conceptualisation: BY. Data curation: BY, MA. Methodology: BY. Investigation: BY, MA, FJ. Formal analysis: BY, MA. Visualisation: BY. Supervision: BY, LM. Original draft: BY. Review & editing: BY, MA, FJ, LM. Funding acquisition: LM.

Ethics statement

The activities of the EstBB are regulated by the Human Genes Research Act, which was adopted in 2000 specifically for the operations of the EstBB. Individual level data analysis was carried out under ethical approval 1.1-12/624 (issued 24.03.2020), 1.1-12/2618 (issued 04.08.2022) and 1.1-12/3454 (issued 20.10.2022) from the Estonian Committee on Bioethics and Human Research (Estonian Ministry of Social Affairs).

References

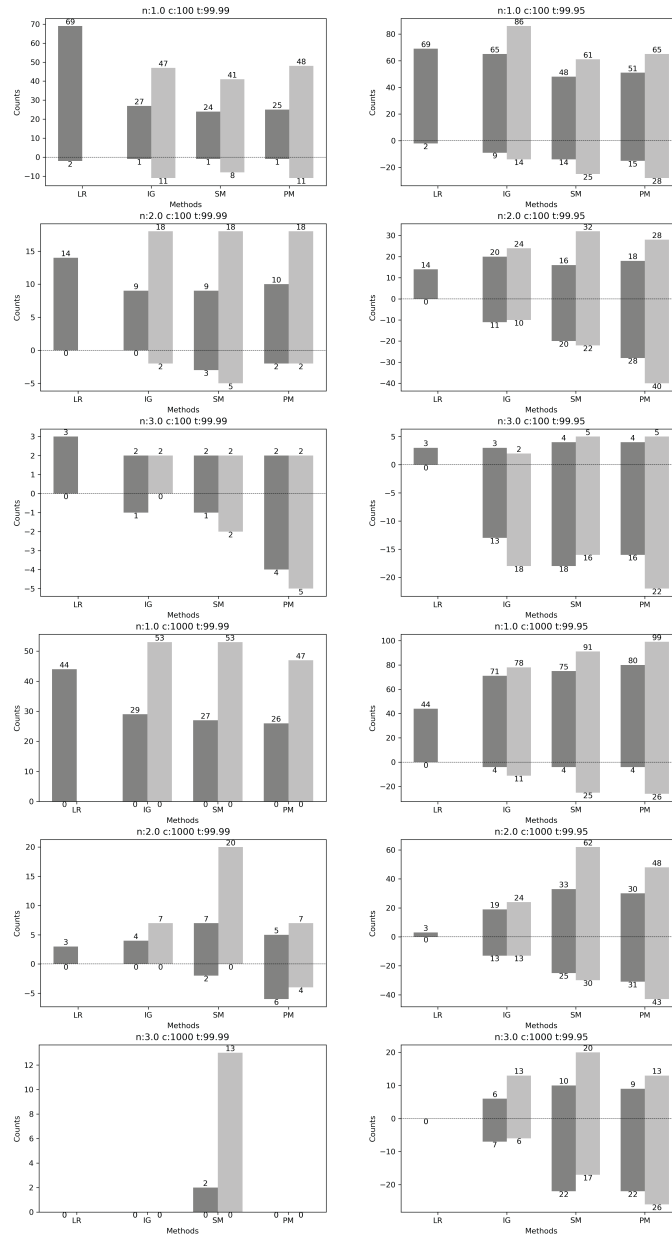
1. A. Abdellaoui, L. Yengo, K. J. H. Verweij, and P. M. Visscher, “15 years of GWAS discovery: Realizing the promise,” *The American Journal of Human Genetics*, vol. 110, pp. 179–194, Feb. 2023.
2. L. Jiang, Z. Zheng, H. Fang, and J. Yang, “A generalized linear mixed model association tool for biobank-scale data,” *Nature Genetics*, vol. 53, pp. 1616–1621, Nov. 2021. Publisher: Nature Publishing Group.
3. J. Mbatchou, L. Barnard, J. Backman, A. Marcketta, J. A. Kosmicki, A. Ziyatdinov, C. Benner, C. O’Dushlaine, M. Barber, B. Boutkov, L. Habegger, M. Ferreira, A. Baras, J. Reid, G. Abecasis, E. Maxwell, and J. Marchini, “Computationally efficient whole-genome regression for quantitative and binary traits,” *Nature Genetics*, vol. 53, pp. 1097–1103, July 2021. Publisher: Nature Publishing Group.
4. Y. Lu and J. Lu, “A universal approximation theorem of deep neural networks for expressing probability distributions,” in *Proceedings of the 34th International Conference on Neural Information Processing Systems*, NIPS ’20, (Red Hook, NY, USA), pp. 3094–3105, Curran Associates Inc., Dec. 2020.
5. W. S. Alharbi and M. Rashid, “A review of deep learning applications in human genomics using next-generation sequencing data,” *Human Genomics*, vol. 16, p. 26, July 2022.
6. X. Zhou, Y. Chen, F. C. F. Ip, Y. Jiang, H. Cao, G. Lv, H. Zhong, J. Chen, T. Ye, Y. Chen, Y. Zhang, S. Ma, R. M. N. Lo, E. P. S. Tong, V. C. T. Mok, T. C. Y. Kwok, Q. Guo, K. Y. Mok, M. Shuai, J. Hardy, L. Chen, A. K. Y. Fu, and N. Y. Ip, “Deep learning-based polygenic risk analysis for Alzheimer’s disease prediction,” *Communications Medicine*, vol. 3, pp. 1–20, Apr. 2023. Publisher: Nature Publishing Group.
7. A. van Hilten, S. A. Kushner, M. Kayser, M. A. Ikram, H. H. H. Adams, C. C. W. Klaver, W. J. Niessen, and G. V. Roshchupkin, “GenNet framework: interpretable deep learning for predicting phenotypes from genetic data,” *Communications Biology*, vol. 4, pp. 1–9, Sept. 2021. Number: 1 Publisher: Nature Publishing Group.
8. J. Xu, C. Mao, Y. Hou, Y. Luo, J. L. Binder, Y. Zhou, L. M. Bekris, J. Shin, M. Hu, F. Wang, C. Eng, T. I. Oprea, M. E. Flanagan, A. A. Pieper, J. Cummings, J. B. Leverenz, and F. Cheng, “Interpretable deep learning translation of GWAS and multi-omics findings to identify pathobiology and drug repurposing in Alzheimer’s disease,” *Cell Reports*, vol. 41, p. 111717, Nov. 2022.
9. L. Liu, Q. Meng, C. Weng, Q. Lu, T. Wang, and Y. Wen, “Explainable deep transfer learning model for disease risk prediction using high-dimensional genomic data,” *PLOS Computational Biology*, vol. 18, p. e1010328, July 2022. Publisher: Public Library of Science.
10. A. Badré and C. Pan, “Explainable multi-task learning improves the parallel estimation of polygenic risk scores for many diseases through shared genetic basis,” *PLOS Computational Biology*, vol. 19, p. e1011211, July 2023. Publisher: Public Library of Science.
11. Y. Liu, D. Wang, F. He, J. Wang, T. Joshi, and D. Xu, “Phenotype Prediction and Genome-Wide Association Study Using Deep Convolutional Neural Network of Soybean,” *Frontiers in Genetics*, vol. 10, 2019.
12. B. Mieth, A. Rozier, J. A. Rodriguez, M. M. C. Höhne, N. Görnitz, and K.-R. Müller, “DeepCOMBI: explainable artificial intelligence for the analysis and discovery in genome-wide association studies,” *NAR Genomics and Bioinformatics*, vol. 3, p. lqab065, Sept. 2021.

13. P. H. Kassani, F. Lu, Y. Le Guen, M. E. Belloy, and Z. He, “Deep neural networks with controlled variable selection for the identification of putative causal genetic variants,” *Nature Machine Intelligence*, vol. 4, pp. 761–771, Sept. 2022. Publisher: Nature Publishing Group.
14. L. Leitsalu, T. Haller, T. Esko, M.-L. Tammesoo, H. Alavere, H. Snieder, M. Perola, P. C. Ng, R. Mägi, L. Milani, K. Fischer, and A. Metspalu, “Cohort Profile: Estonian Biobank of the Estonian Genome Center, University of Tartu,” *International Journal of Epidemiology*, vol. 44, pp. 1137–1147, Aug. 2015.
15. D. Ho, K. Imai, G. King, and E. A. Stuart, “MatchIt: Nonparametric Preprocessing for Parametric Causal Inference,” *Journal of Statistical Software*, vol. 42, pp. 1–28, June 2011.
16. M. Buda, A. Maki, and M. A. Mazurowski, “A systematic study of the class imbalance problem in convolutional neural networks,” *Neural Networks*, vol. 106, pp. 249–259, Oct. 2018.
17. A. Paszke, S. Gross, F. Massa, A. Lerer, J. Bradbury, G. Chanan, T. Killeen, Z. Lin, N. Gimelshein, L. Antiga, A. Desmaison, A. Köpf, E. Yang, Z. DeVito, M. Raison, A. Tejani, S. Chilamkurthy, B. Steiner, L. Fang, J. Bai, and S. Chintala, “PyTorch: An Imperative Style, High-Performance Deep Learning Library,” Dec. 2019. arXiv:1912.01703 [cs, stat].
18. K. Simonyan, A. Vedaldi, and A. Zisserman, “Deep Inside Convolutional Networks: Visualising Image Classification Models and Saliency Maps,” Apr. 2014. arXiv:1312.6034 [cs].
19. M. Sundararajan, A. Taly, and Q. Yan, “Axiomatic attribution for deep networks,” in *Proceedings of the 34th International Conference on Machine Learning - Volume 70, ICML’17*, (Sydney, NSW, Australia), pp. 3319–3328, JMLR.org, Aug. 2017.
20. N. Kokhlikyan, V. Miglani, M. Martin, E. Wang, B. Alsallakh, J. Reynolds, A. Melnikov, N. Kliushkina, C. Araya, S. Yan, and O. Reblitz-Richardson, “Captum: A unified and generic model interpretability library for PyTorch,” 2020. eprint: 2009.07896.
21. L. Breiman, “Random Forests,” *Machine Learning*, vol. 45, pp. 5–32, Oct. 2001.
22. M. J. Owen, “Genomic insights into schizophrenia,” *Royal Society Open Science*, vol. 10, p. 230125, Feb. 2023. Publisher: Royal Society.
23. S. Seabold and J. Perktold, “statsmodels: Econometric and statistical modeling with python,” in *9th Python in Science Conference*, 2010.
24. N. Pujol Gualdo, Estonian Biobank Research Team, R. Mägi, and T. Laisk, “Genome-wide association study meta-analysis supports association between MUC1 and ectopic pregnancy,” *Human Reproduction*, vol. 38, pp. 2516–2525, Dec. 2023.
25. S. Rao, A. Baranova, Y. Yao, J. Wang, and F. Zhang, “Genetic Relationships between Attention-Deficit/Hyperactivity Disorder, Autism Spectrum Disorder, and Intelligence,” *Neuropsychobiology*, vol. 81, pp. 484–496, June 2022.
26. M. Lam, W. D. Hill, J. W. Trampush, J. Yu, E. Knowles, G. Davies, E. Stahl, L. Huckins, D. C. Liewald, S. Djurovic, I. Melle, K. Sundet, A. Christoforou, I. Reinvang, P. DeRosse, A. J. Lundervold, V. M. Steen, T. Espeseth, K. Räikkönen, E. Widen, A. Palotie, J. G. Eriksson, I. Giegling, B. Konte, A. M. Hartmann, P. Roussos, S. Giakoumaki, K. E. Burdick, A. Payton, W. Ollier, O. Chiba-Falek, D. K. Attix, A. C. Need, E. T. Cirulli, A. N. Voineskos, N. C. Stefanis, D. Avramopoulos, A. Hatzimanolis, D. E. Arking, N. Smyrnis, R. M. Bilder, N. A. Freimer, T. D. Cannon, E. London, R. A. Poldrack, F. W. Sabb, E. Congdon, E. D. Conley, M. A. Scult, D. Dickinson, R. E. Straub, G. Donohoe, D. Morris, A. Corvin, M. Gill, A. R. Hariri, D. R. Weinberger, N. Pendleton, P. Bitsios, D. Rujescu, J. Lahti, S. Le Hellard, M. C. Keller, O. A. Andreassen, I. J. Deary, D. C. Glahn, A. K. Malhotra, and T. Lencz, “Pleiotropic Meta-Analysis

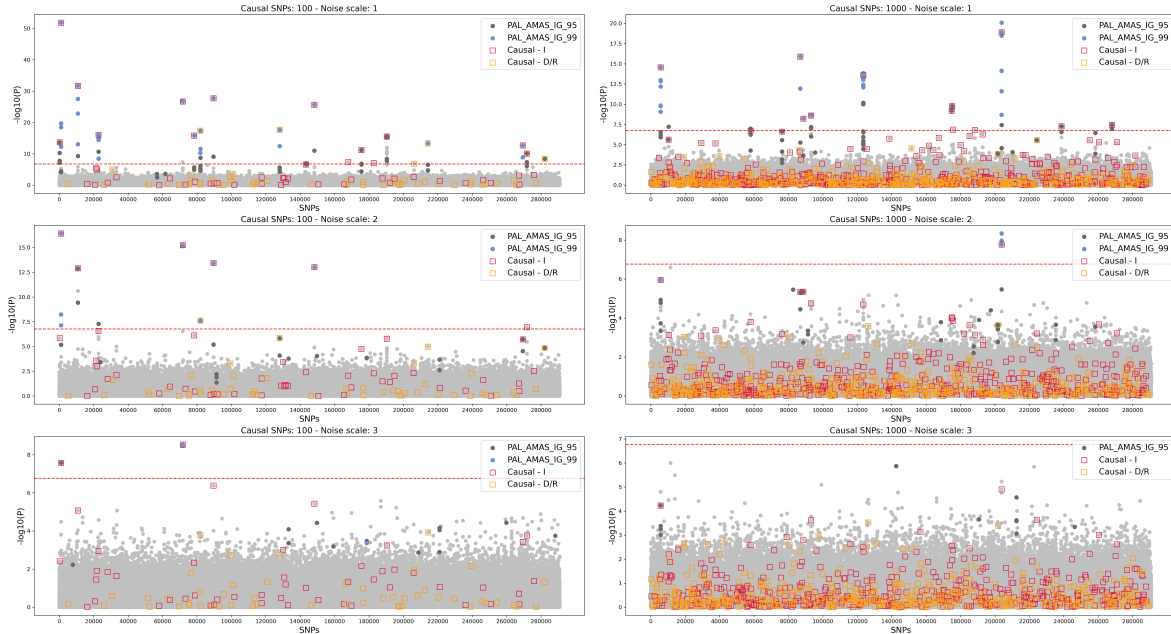
- of Cognition, Education, and Schizophrenia Differentiates Roles of Early Neurodevelopmental and Adult Synaptic Pathways,” *The American Journal of Human Genetics*, vol. 105, pp. 334–350, Aug. 2019.
27. V. Trubetsky, A. F. Pardiñas, T. Qi, *et al.*, “Mapping genomic loci implicates genes and synaptic biology in schizophrenia,” *Nature*, vol. 604, pp. 502–508, Apr. 2022. Publisher: Nature Publishing Group.
 28. N. Mullins, A. J. Forstner, K. S. O’Connell, *et al.*, “Genome-wide association study of more than 40,000 bipolar disorder cases provides new insights into the underlying biology,” *Nature Genetics*, vol. 53, pp. 817–829, June 2021. Publisher: Nature Publishing Group.
 29. E. A. Stahl, G. Breen, A. J. Forstner, *et al.*, “Genome-wide association study identifies 30 loci associated with bipolar disorder,” *Nature Genetics*, vol. 51, pp. 793–803, May 2019. Publisher: Nature Publishing Group.
 30. P. Turley, R. K. Walters, O. Maghzian, A. Okbay, J. J. Lee, M. A. Fontana, T. A. Nguyen-Viet, R. Wedow, M. Zacher, N. A. Furlotte, P. Magnusson, S. Oskarsson, M. Johannesson, P. M. Visscher, D. Laibson, D. Cesarini, B. M. Neale, and D. J. Benjamin, “Multi-trait analysis of genome-wide association summary statistics using MTAG,” *Nature Genetics*, vol. 50, pp. 229–237, Feb. 2018. Publisher: Nature Publishing Group.
 31. B. M. L. Baselmans, R. Jansen, H. F. Ip, J. van Dongen, A. Abdellaoui, M. P. van de Weijer, Y. Bao, M. Smart, M. Kumari, G. Willemsen, J.-J. Hottenga, D. I. Boomsma, E. J. C. de Geus, M. G. Nivard, and M. Bartels, “Multivariate genome-wide analyses of the well-being spectrum,” *Nature Genetics*, vol. 51, pp. 445–451, Mar. 2019. Publisher: Nature Publishing Group.
 32. D. F. Levey, M. B. Stein, F. R. Wendt, G. A. Pathak, H. Zhou, M. Aslan, R. Quaden, K. M. Harrington, Y. Z. Nuñez, C. Overstreet, K. Radhakrishnan, G. Sanacora, A. M. McIntosh, J. Shi, S. S. Shringarpure, J. Concato, R. Polimanti, and J. Gelernter, “Bi-ancestral depression GWAS in the Million Veteran Program and meta-analysis in >1.2 million individuals highlight new therapeutic directions,” *Nature Neuroscience*, vol. 24, pp. 954–963, July 2021. Publisher: Nature Publishing Group.
 33. X. Meng, G. Navoly, O. Giannakopoulou, D. F. Levey, D. Koller, G. A. Pathak, N. Koen, K. Lin, M. J. Adams, M. E. Rentería, Y. Feng, J. M. Gaziano, D. J. Stein, H. J. Zar, M. L. Campbell, D. A. van Heel, B. Trivedi, S. Finer, A. McQuillin, N. Bass, V. K. Chundru, H. C. Martin, Q. Q. Huang, M. Valkovskaya, C.-Y. Chu, S. Kanjira, P.-H. Kuo, H.-C. Chen, S.-J. Tsai, Y.-L. Liu, K. S. Kendler, R. E. Peterson, N. Cai, Y. Fang, S. Sen, L. J. Scott, M. Burmeister, R. J. F. Loos, M. H. Preuss, K. V. Actkins, L. K. Davis, M. Uddin, A. H. Wani, D. E. Wildman, A. E. Aiello, R. J. Ursano, R. C. Kessler, M. Kanai, Y. Okada, S. Sakaue, J. A. Rabinowitz, B. S. Maher, G. Uhl, W. Eaton, C. S. Cruz-Fuentes, G. A. Martinez-Levy, A. I. Campos, I. Y. Millwood, Z. Chen, L. Li, S. Wassertheil-Smoller, Y. Jiang, C. Tian, N. G. Martin, B. L. Mitchell, E. M. Byrne, S. Awasthi, J. R. I. Coleman, S. Ripke, T. Sofer, R. G. Walters, A. M. McIntosh, R. Polimanti, E. C. Dunn, M. B. Stein, J. Gelernter, C. M. Lewis, and K. Kuchenbaecker, “Multi-ancestry genome-wide association study of major depression aids locus discovery, fine mapping, gene prioritization and causal inference,” *Nature Genetics*, vol. 56, pp. 222–233, Feb. 2024. Publisher: Nature Publishing Group.
 34. T. D. Als, M. I. Kurki, J. Grove, G. Voloudakis, K. Therrien, E. Tasanko, T. T. Nielsen, J. Naamanka, K. Veerapen, D. F. Levey, J. Bendl, J. Bybjerg-Grauholm, B. Zeng, D. Demontis, A. Rosengren, G. Athanasiadis, M. Bækved-Hansen, P. Qvist, G. Bragi Walters, T. Thorgeirsson, H. Stefánsson, K. L. Musliner, V. M. Rajagopal, L. Farajzadeh, J. Thirstrup, B. J. Vilhjálmsson, J. J. McGrath, M. Mattheisen, S. Meier, E. Agerbo, K. Stefánsson, M. Nordentoft, T. Werge, D. M. Hougaard, P. B. Mortensen, M. B. Stein, J. Gelernter, I. Hovatta, P. Roussos, M. J. Daly,

- O. Mors, A. Palotie, and A. D. Børglum, “Depression pathophysiology, risk prediction of recurrence and comorbid psychiatric disorders using genome-wide analyses,” *Nature Medicine*, vol. 29, pp. 1832–1844, July 2023. Publisher: Nature Publishing Group.
35. A. J. Schork, H. Won, V. Appadurai, R. Nudel, M. Gandal, O. Delaneau, M. Revsbech Christiansen, D. M. Hougaard, M. Bækved-Hansen, J. Bybjerg-Grauholm, M. Giørtz Pedersen, E. Agerbo, C. Bøcker Pedersen, B. M. Neale, M. J. Daly, N. R. Wray, M. Nordentoft, O. Mors, A. D. Børglum, P. Bo Mortensen, A. Buil, W. K. Thompson, D. H. Geschwind, and T. Werge, “A genome-wide association study of shared risk across psychiatric disorders implicates gene regulation during fetal neurodevelopment,” *Nature Neuroscience*, vol. 22, pp. 353–361, Mar. 2019. Publisher: Nature Publishing Group.
36. J. Kaplanis, N. Akawi, G. Gallone, J. F. McRae, E. Prigmore, C. F. Wright, D. R. Fitzpatrick, H. V. Firth, J. C. Barrett, M. E. Hurles, and o. b. o. t. D. D. D. Study, “Exome-wide assessment of the functional impact and pathogenicity of multinucleotide mutations,” *Genome Research*, vol. 29, pp. 1047–1056, July 2019. Company: Cold Spring Harbor Laboratory Press Distributor: Cold Spring Harbor Laboratory Press Institution: Cold Spring Harbor Laboratory Press Label: Cold Spring Harbor Laboratory Press Publisher: Cold Spring Harbor Lab.
37. Y. Chen, W. Li, L. Lv, and W. Yue, “Shared Genetic Determinants of Schizophrenia and Autism Spectrum Disorder Implicate Opposite Risk Patterns: A Genome-Wide Analysis of Common Variants,” *Schizophrenia Bulletin*, p. sbae044, Apr. 2024.
38. F. Aguet, A. A. Brown, S. E. Castel, *et al.*, “Genetic effects on gene expression across human tissues,” *Nature*, vol. 550, pp. 204–213, Oct. 2017. Publisher: Nature Publishing Group.
39. K. Watanabe, E. Taskesen, A. van Bochoven, and D. Posthuma, “Functional mapping and annotation of genetic associations with FUMA,” *Nature Communications*, vol. 8, p. 1826, Nov. 2017. Publisher: Nature Publishing Group.
40. E. Candès, Y. Fan, L. Janson, and J. Lv, “Panning for Gold: ‘Model-X’ Knockoffs for High Dimensional Controlled Variable Selection,” *Journal of the Royal Statistical Society Series B: Statistical Methodology*, vol. 80, pp. 551–577, June 2018.
41. E. A. Boyle, Y. I. Li, and J. K. Pritchard, “An Expanded View of Complex Traits: From Polygenic to Omnigenic,” *Cell*, vol. 169, pp. 1177–1186, June 2017.

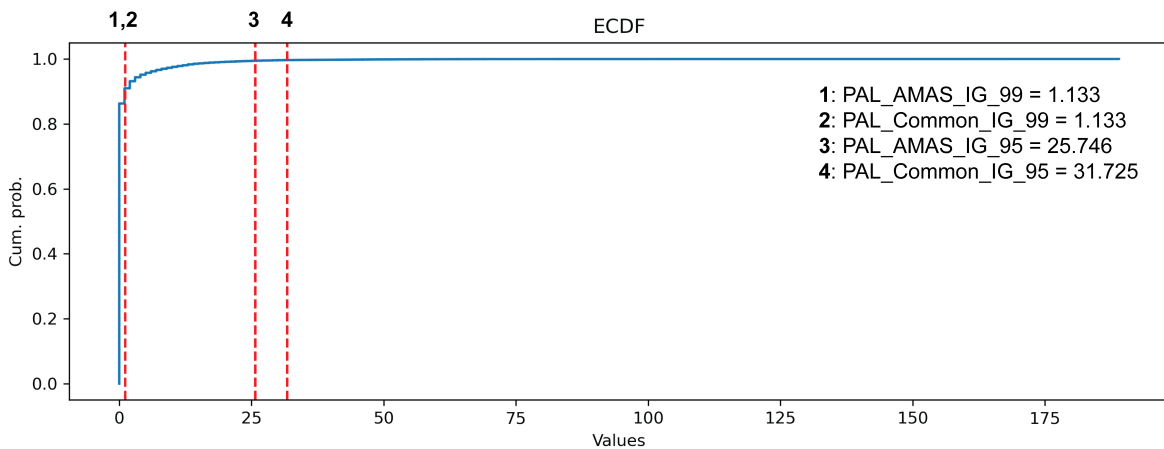
Supplementary Figures



S1 Fig. Comparison of true positive (TP) and false positive (FP) counts for different methods based on various simulation scenarios and thresholding (n : noise factor, c : number of causal positions, t : significance threshold). TP was defined as a detected position which is in high correlation ($r^2 > 0.5$ in 100 SNP upstream and 100 SNP downstream region, total $\sim 2\text{Mb}$) with any true causal position. Positive values (above 0 on the y-axis) indicate TP counts whereas negative values (below 0 on the y-axis) indicate FP counts. Methods defined in x-axis are logistic regression (LR), integrated gradients (IG), saliency map (SM) and permutation-based (PM) approaches. For IG, SM and PM, the first bar (dark grey) shows TP/FP counts for *PALAMAS* whereas the second bar (light grey) shows TP/FP counts for *PALCommon*. For LR, TP/FP counts were obtained based on significant signals obtained with Bonferroni correction (i.e., $p\text{-value} = 0.05$ divided by the number of tests).

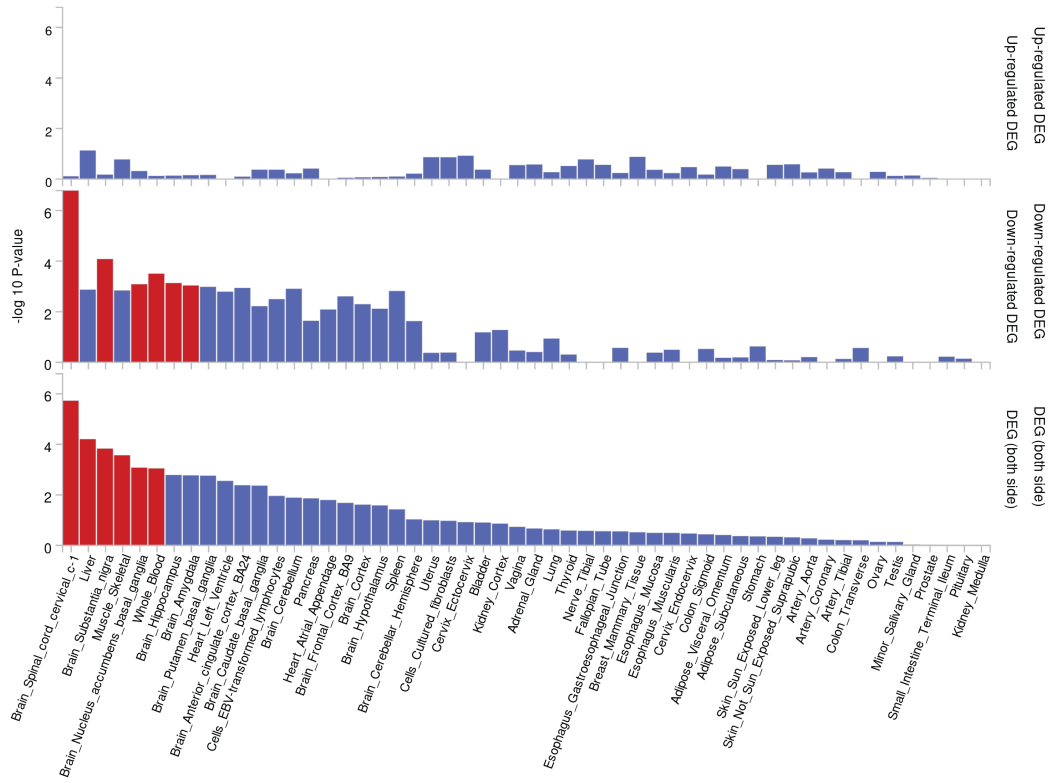


S2 Fig. Manhattan plots from LR with annotated PAL_{AMAS} detected via IG approach. x-axis denotes SNP positions over the whole genome, and y-axis denotes $-\log(P)$ values. Each figure is a different simulation scenario with varying amounts of noise and causal SNPs, as described in the subcaptions. Dashed red lines denote the significance threshold for LR (with Bonferroni corrected p-value = 0.05 divided by the number of tests). Red squares denote causal SNPs with interactive effects (Causal - I), and orange squares denote causal SNPs with dominant/recessive effects (Causal - D/R). Blue and black dots represent PAL_{AMAS} detected with strict (99.99 percentile) and relaxed (99.95 percentile) thresholds, respectively.

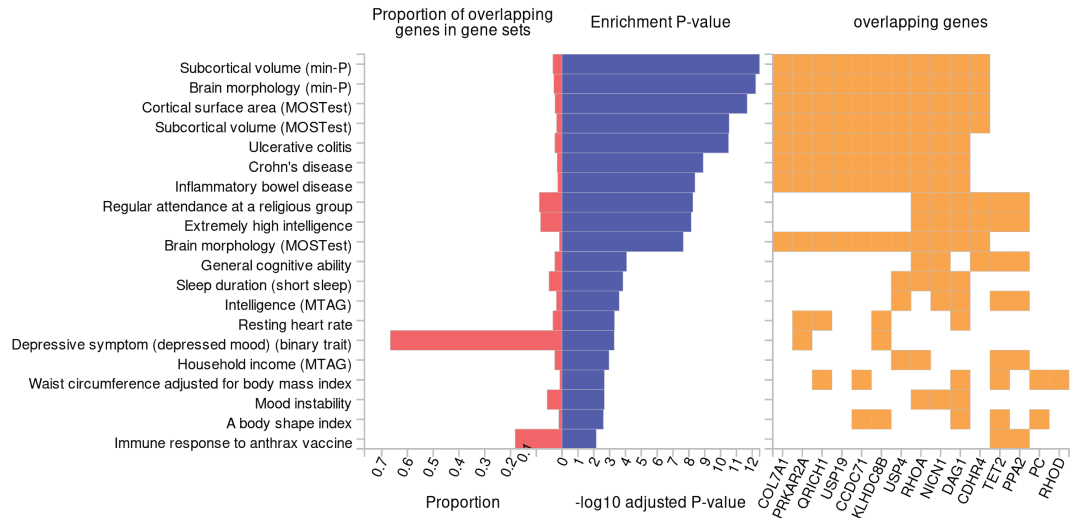


S3 Fig. Empirical cumulative distribution function (ECDF) plot of brain tissue expression for all 290,522 SNPs. Values (x-axis) correspond to the number of gene-tissue (consisting of all types of brain tissues) combinations with significant expression change. Numbers correspond to the average values for SNPs in PAL detected with different methods and parameters. Percentile ranks from 1 to 4 are 0.910, 0.910, 0.994 and 0.996, respectively.

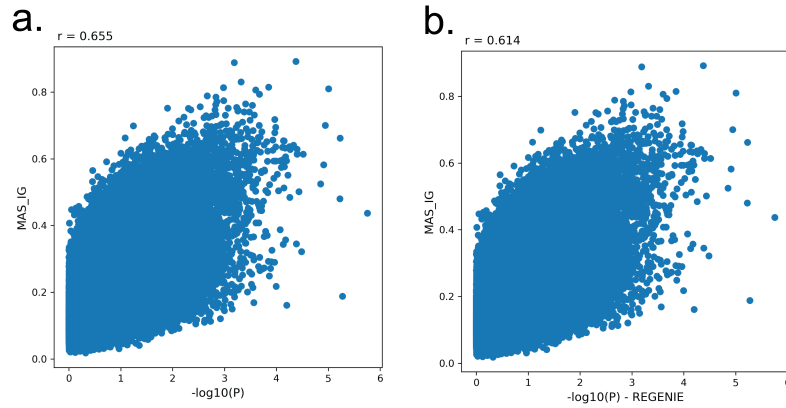
a.



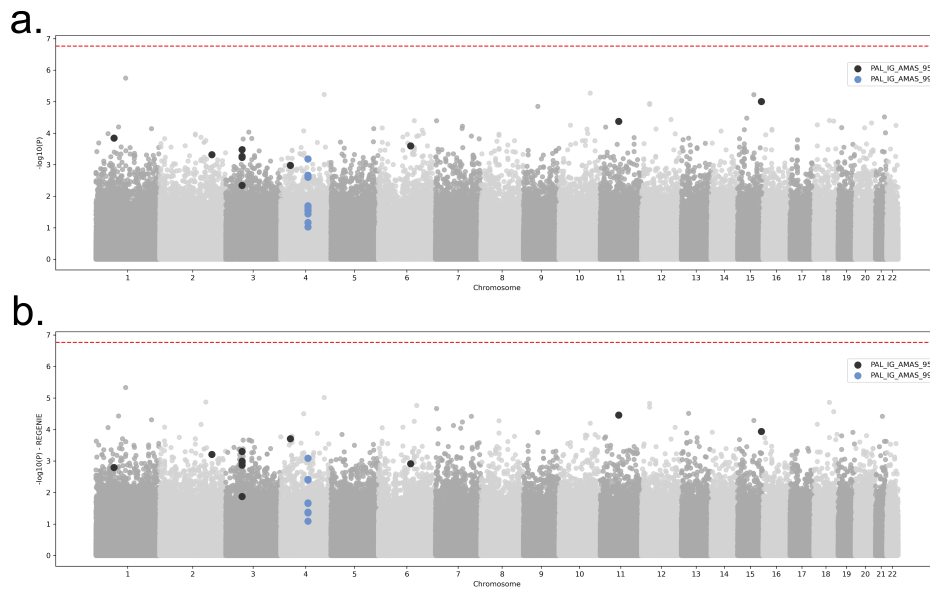
b.



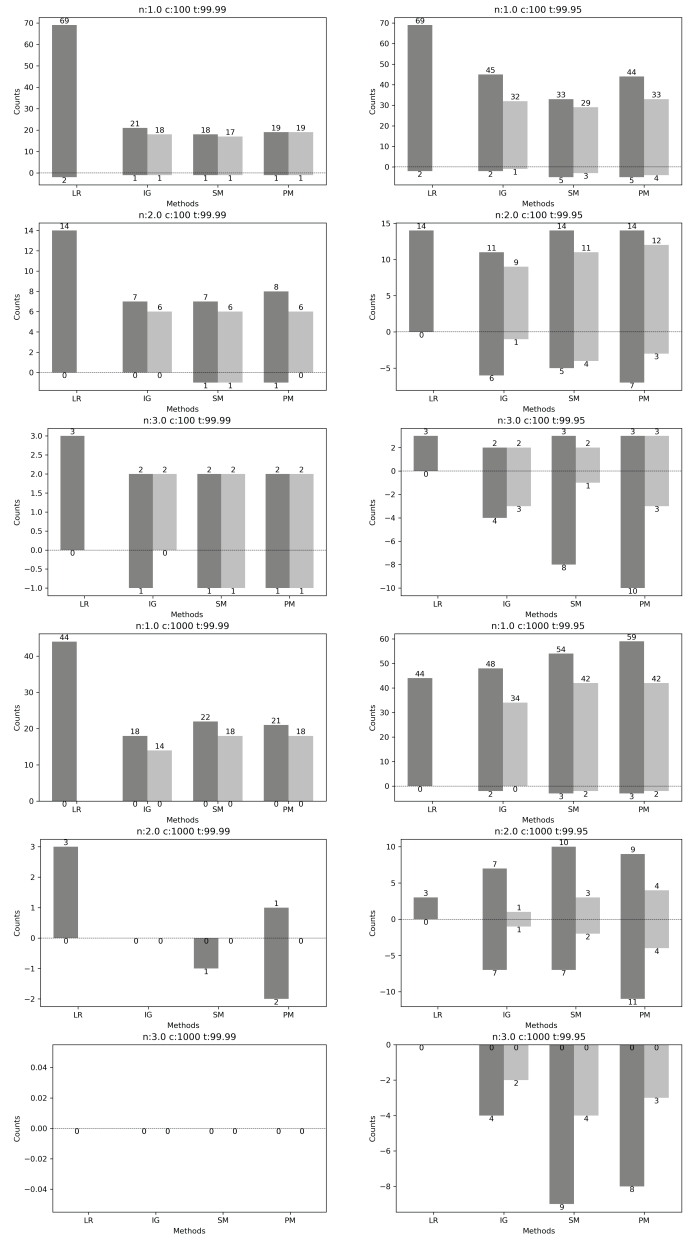
S4 Fig. FUMA functional analysis of detected genes. **a)** Differentially expressed gene (DEG) sets with significant enrichments based on Bonferroni correction coloured in red. **b)** Enrichment in GWAS-catalogue gene sets.



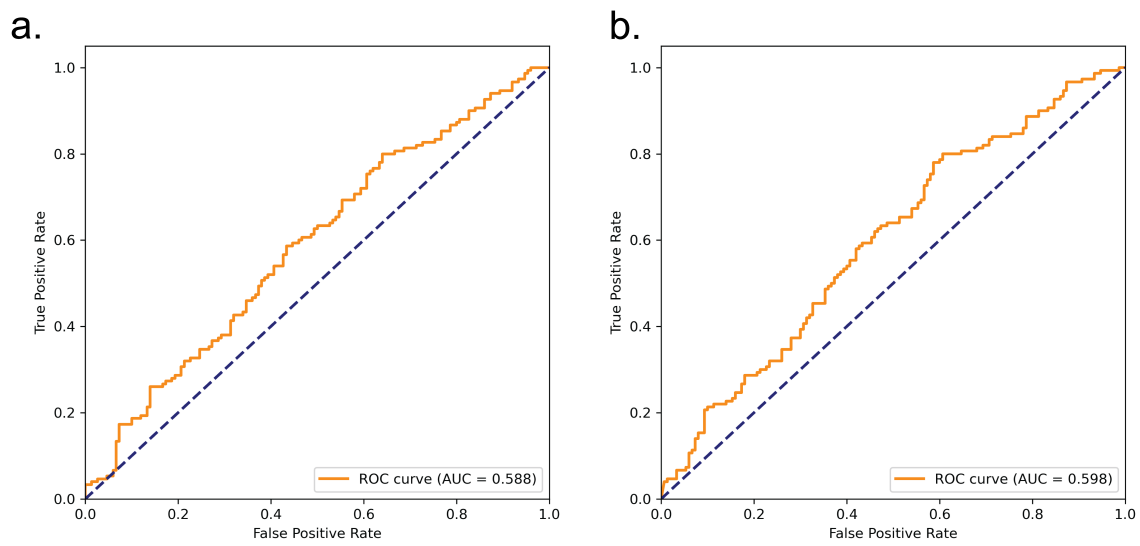
S5 Fig. Correlation between mean attribution score (averaged over 10 different models) obtained via integrated gradient (MAS_IG) approach and $-\log(P)$ values obtained via **a)** logistic regression and **b)** REGENIE association analysis using SCZ dataset. Provided r values are Pearson's correlation coefficient.



S6 Fig. Manhattan plots from **a)** LR and **b)** REGENIE association analysis with annotated PAL_{AMAS} detected via IG approach for SCZ dataset. Blue and black dots represent PAL_{AMAS} detected with strict (99.99 percentile) and relaxed (99.95 percentile) thresholds, respectively. Red dashed lines show significance thresholds for LR and REGENIE analyses.



S7 Fig. Comparison of true positive (TP) and false positive (FP) counts for different methods based on various simulation scenarios and thresholding (n: noise factor, c: number of causal positions, t: significance threshold). For neural network-based methods, only exact detected SNPs were considered as common between models (see Discussion). TP was defined as a detected position which is in high correlation ($r^2 > 0.5$ in 100 SNP upstream and 100 SNP downstream region, total ~2Mb) with any true causal position. Positive values (above 0 on the y-axis) indicate TP counts, whereas negative values (below 0 on the y-axis) indicate FP counts. Methods defined in the x-axis are logistic regression (LR), integrated gradients (IG), saliency map (SM) and permutation-based (PM) approaches. For IG, SM and PM, the first bar (dark grey) shows TP/FP counts for *PALAMAS* whereas the second bar (light grey) shows TP/FP counts for *PALCommon*. For LR, TP/FP counts were obtained based on significant signals obtained with Bonferroni correction (i.e., p-value = 0.05 divided by the number of tests).



S8 Fig. Receiver operating characteristic (ROC) curves and area under the ROC curve (AUC) for **a)** neural network models trained for 1000 epochs (predictions averaged over 10 models trained with different seeds) and **b)** logistic regression phenotype predictions. Predictions were performed on the same test genotypes (150 cases, 150 controls) not utilised in fitting or training.